Int. J. Multiphase Flow Vol. 17, No. 5, pp. 661–676, 1991
Printed in Great Britain.

0301-9322/91 $3.00 + 0.00

AN APPROXIMATE ANALYTICAL SOLUTION OF THE HYDRODYNAMIC PROBLEM ASSOCIATED WITH AN ADVANCING LIQUID–GAS CONTACT LINE

W. BOENDER,† A. K. CHESTERS and A. J. J. VAN DER ZANDEN
Laboratory of Fluid Dynamics and Heat Transfer, Eindhoven University of Technology, P.O. Box 513, Eindhoven, The Netherlands

(Received 1 July 1990; in revised form 21 April 1991)

Abstract—An alternative to perturbation techniques or full numerical solution is developed for the free-surface problem associated with an advancing liquid–gas contact line. The method, which makes use of a local-wedge approximation to obtain the free-surface pressure variation, leads to a second-order ordinary differential equation for the meniscus shape. Both analytical considerations and comparisons with available full numerical solutions for capillary tubes confirm the validity of the meniscus equation up to values of the capillary number (Ca) of order 10^{-1}. At higher Ca the equation retains its validity in the wall region, for which an approximate analytical solution is derived. Matching of this solution with the central circular meniscus profile leads to an analytical approximation for the advancing contact angle, which compares excellently with available data (Ca up to an order 1). In contrast with preceding analyses, the classical approximations—in particular, that of no slip—are assumed to retain their validity up to the order of a molecular dimension from the wall, at which point the true contact angle is reached. While this angle is again supposed to be equal to the static value, this assumption is not critical to the dynamic angle predicted.

Key Words: wetting, dynamic contact line

1. INTRODUCTION

In macroscopic static systems involving three-phase contact lines the contact angle constitutes an essential boundary condition, whose value on smooth, chemically homogeneous solids depends only on the media involved and not on system parameters.

It is appealing to extend the concept of contact angle to the dynamic case, in which the three-phase line moves over the solid and the "dynamic" contact angle in the advancing fluid is observed to be an increasing function of the line speed. Even in the simplest case, considered here, of a viscous liquid steadily displacing a gas, one of the problems encountered is that whatever the value of the dynamic contact angle the associated flow field proves to be singular, the pressure in the liquid decreasing without limit as the line is approached if the "classical" approximations of fluid mechanics are retained: that the liquid is a continuum, possessing a surface tension and subject to no slip with respect to the solid. This dilemma does, however, provide the first clue as to the origin of the dynamic contact angle, namely that at least part of the deviation from the static angle must be apparent rather than real, resulting from deformation of the meniscus in a microscopic region close to the line where the pressure in the advancing fluid is very low [for relatively recent reviews, see Dussan (1979) and de Gennes (1985)]. The problem of the singularity remains, however, the magnitude of the deviation from the static angle being unlimited if the classical approximations are retained. It thus appears that the breakdown of one or more of these aproximations extremely close to the wall must be taken into account in any complete description of the phenomena.

Even aside from the question of the appropriate wall boundary conditions, the problem of finding the meniscus shape is a difficult one and most solutions to date are based on perturbation techniques, valid only for small values of the capillary number (Ca), $\mu U/\sigma$ (μ—dynamic viscosity

†Present address: Hoogovens Research Laboratory, P.O. Box 10,000, IJmuiden, The Netherlands.

of the liquid, U—line speed, σ—surface tension): Hansen & Toong (1971), Voinov (1976), Huh & Mason (1977), Greenspan (1978), Voinov (1978), Kakfa & Dussan (1979), Neogi & Miller (1982), Hocking & Rivers (1982) and Cox (1986). Direct numerical (finite-element) solutions up to a Ca of almost 10^{-1} have, however, been obtained by Lowndes (1980). Of the preceding authors, all but Voinov coped with the wall boundary condition by assuming the no-slip approximation to break down while retaining the continuum description and the idealization of surface tension. In addition, they assumed the true contact angle to remain unchanged and equal to the static value. Lowndes' (1980) results exhibited good agreement with the dynamic contact angles measured by Hoffman (1975) if the size of the region in which slip was significant was taken to be of the order of a molecular dimension (1 nm). This result suggests of course that non-continuum effects *are* likely to be significant, if not dominant.

The primary contribution of the present paper is to develop an alternative approximation to perturbation techniques for the solution of the advancing meniscus shape in that domain of the wall region in which the classical approximations apply. The approach is based on the solution of the creeping flow and pressure field in the case of a free surface of constant inclination (Moffatt, 1964). This solution should be locally applicable, even at large values of Ca, provided the actual inclination changes only slowly (in some appropriate dimensionless sense), much as the Poiseuille equation for pressure drop in a tube would be, provided the tube diameter changed slowly. This approach yields a second-order ordinary differential equation for the meniscus shape which can either be solved numerically or, with the help of suitable further approximations, analytically.

To make use of the resulting meniscus equation to predict dynamic contact angles some assumption is again required as to the wall boundary condition. In contrast with preceding authors, excepting Voinov, the possibility is explored that the continuum, rather than the no-slip, approximation must be abandoned. Specifically, the classical approximations are supposed to apply up to a distance from the wall of the order of a molecular dimension, at which point the wall has been reached and with it the true contact angle. Like previous authors, the simplest assumption is made regarding the true contact angle—that this angle remains unchanged and equal to its static value. This assumption, which has been challenged by various authors (e.g. Hoffman 1983), is not however as critical as it might seem, since even a considerable line-speed-dependence of the true angle proves hardly to affect the dynamic angle in the advancing case.

In section 2 the meniscus equation is derived for the plane-symmetric case, which should apply in all systems at distances from the wall which are small in comparison with the system length scale and conceivably over the entire meniscus in the case of a parallel-plate geometry. The effect of curvature in a plane perpendicular to the flow is then included (section 3), extending the equation to flow in a capillary tube. In the following two sections numerical solutions of these equations are presented for plane-parallel and axi-symmetric cases. In section 6 the axi-symmetric solutions are compared with the finite-element results of Lowndes (1980), agreement being required except in a region of molecular dimensions adjacent to the wall, where the different boundary conditions (slip vs a non-continuum assumption) should make their presence felt.

The broad credentials of the meniscus equation having been established, attention is now directed to its solution with the help of approximate analytical techniques, leading to an analytical approximation for the advancing dynamic contact angle. The first step in this process (section 7) is to derive a solution of the plane meniscus equation (valid in the wall region) in the small-Ca limit. This solution is then shown to provide a good approximation at *all* Ca if Ca is replaced by f(Ca), where f is a simple function reducing to Ca in the small-Ca limit. The accuracy of this solution is checked by comparison with direct numerical integrations of the original meniscus equation. To arrive at predictions of the dynamic contact angle, the analytical solution for the wall region must now be matched with the approximately undeformed meniscus in the centre of the duct (section 8). The simplest matching procedure is found to yield satisfactory results, as indicated by a comparison with Hoffman's (1975) measurements of advancing dynamic angles (up to Ca of order 1: section 9). This comparison also provides a check on the expectation underlying the model: that the value of the distance at which the wall is effectively reached should be of the order of a molecular dimension.

2. THE SHAPE OF AN ADVANCING MENISCUS BETWEEN PLANE-PARALLEL PLATES

The stream function Ψ of a creeping liquid flow in a plane wedge, with a constant velocity U prescribed on one boundary and a free surface (zero shear stress) on the other, has been given by Moffatt (1964), in the coordinates θ and ρ, as

$$\Psi = U\rho \frac{\theta \cos\theta \sin\alpha - \alpha \cos\alpha \sin\theta}{\sin\alpha \cos\alpha - \alpha}, \quad [1]$$

where α is the angle of the wedge (see figure 1). The corresponding deviatoric component of the normal stress in the liquid at the free surface is readily shown to be zero, while the pressure p in the liquid varies along the free surface as

$$\frac{dp}{d\rho} = \frac{\mu U A(\alpha)}{\rho^2}, \quad [2]$$

where μ is the viscosity of the liquid and

$$A(\alpha) = \frac{-2\sin\alpha}{\sin\alpha\cos\alpha - \alpha}. \quad [3]$$

An advancing meniscus between two parallel plates may be described by the coordinates r and φ (figure 2). In this case the wedge angle φ is not constant but varies along the meniscus. However, provided that the stresses exerted by the receding gas on the liquid are negligible (aside from a uniform pressure, taken for simplicity to be zero), the flow is assumed locally to resemble that in a plane wedge (with $\alpha = \varphi$). More precisely, the pressure gradient dp/ds (where s denotes arc length along the meniscus) will be approximated by the pressure gradient $dp/d\rho$ at the free surface of the corresponding plane wedge:

$$\frac{dp}{ds} = \frac{\mu U A(\varphi)}{r^2}. \quad [4]$$

Denoting the distance to the wall by x (figure 2), [4] may be rewritten as

$$\frac{dp}{dx} = \frac{\mu U A(\varphi)\sin\varphi}{x^2}. \quad [5]$$

The normal stress, $-p$, exerted by the liquid, is balanced by the surface tension σ, according to Laplace's law:

$$-p = \frac{\sigma}{R} = \sigma\frac{d\varphi}{ds} = \sigma\sin\varphi\frac{d\varphi}{dx}, \quad [6]$$

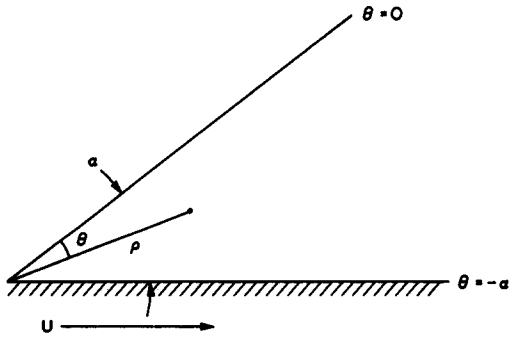

Figure 1. Viscous flow in a plane wedge bounded by a solid with velocity U ($\theta = -\alpha$) and a free surface ($\theta = 0$).

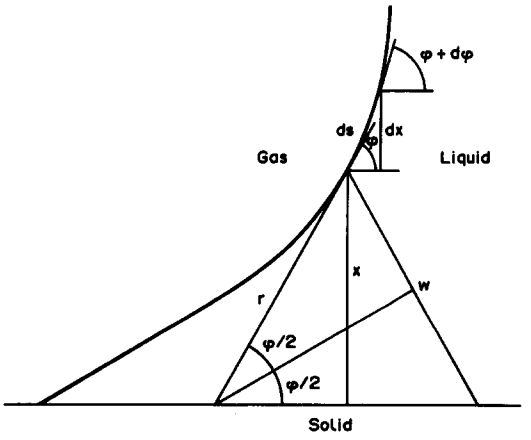

Figure 2. Definition of variables for an advancing meniscus.

where R is the radius of curvature of the meniscus (reckoned positive if the centre of curvature lies on the gas side). The derivative of [6] substituted in [5] now gives

$$\frac{1}{A(\varphi)\sin\varphi}\frac{\mathrm{d}}{\mathrm{d}x}\left(\sin\varphi\frac{\mathrm{d}\varphi}{\mathrm{d}x}\right)=\frac{-\mathrm{Ca}}{x^2}, \qquad [7]$$

in which Ca is the capillary number;

$$\mathrm{Ca}=\frac{\mu U}{\sigma}. \qquad [8]$$

The description of the shape of a moving meniscus between parallel planes by the ordinary differential equation [7] is as good as approximation [4]. The first correction to this approximation would involve some dimensionless local curvate of the wedge, e.g. $(\mathrm{d}\varphi/\varphi)/(\mathrm{d}s/w)$, where w denotes the local wedge width (figure 2). Accordingly, [4] may be expected to be acceptable provided

$$\frac{\dfrac{\mathrm{d}\varphi}{\varphi}}{\dfrac{\mathrm{d}s}{w}}\ll 1. \qquad [9]$$

3. THE SHAPE OF AN ADVANCING MENISCUS IN A CAPILLARY

Unlike the case of parallel plates, the flow behind an advancing meniscus in a capillary tube is no longer two-dimensional, though close to the wall (the region where viscous stresses make the meniscus deviate noticeably from a sphere) [5] still provides a good description of the pressure gradient. Because the meniscus is no longer cylindrical, the pressure behind the advancing meniscus is balanced by two radii of curvature:

$$-p=\sigma\left(\frac{1}{R_1}+\frac{1}{R_2}\right), \qquad [10]$$

where R_1 is the radius of curvature in the plane of figure 3 and R_2 in the plane normal to it; R_1 is given (as in [6]) by

$$\frac{1}{R_1}=\sin\varphi\frac{\mathrm{d}\varphi}{\mathrm{d}x} \qquad [11]$$

and R_2 by

$$\frac{a-x}{-R_2}=\cos(\pi-\varphi)=-\cos\varphi, \qquad [12]$$

where a is the tube radius (see figure 3). From [5], [10], [11] and [12] the new meniscus equation is obtained:

$$\frac{\mathrm{d}}{\mathrm{d}x}\left(\sin\varphi\frac{\mathrm{d}\varphi}{\mathrm{d}x}+\frac{\cos\varphi}{a-x}\right)=\frac{-\mathrm{Ca}\,A(\varphi)\sin\varphi}{x^2}. \qquad [13]$$

4. THE NUMERICAL SOLUTION OF THE MENISCUS EQUATION IN THE PLANE CASE

Equation [7] cannot be valid for all x, since this equation is based on [1] and [6], which treat the liquid as a continuum, bounded by an infinitesimally thin surface possessing a tension. While this is an acceptable approximation on a macroscopic and microscopic scale, on a "nanoscopic" scale, of the order of molecular dimensions, it is certainly not. The distance from the wall beneath which [7] is no longer valid will be denoted by λ.

Defining the logarithmic scale of distance

$$\xi = \ln\left(\frac{x}{\lambda}\right), \qquad [14]$$

[7] becomes

$$\frac{1}{A(\varphi)\sin\varphi}\frac{\mathrm{d}}{\lambda\exp(\xi)\,\mathrm{d}\xi}\left[\sin\varphi\frac{\mathrm{d}\varphi}{\lambda\exp(\xi)\,\mathrm{d}\xi}\right] = \frac{-\mathrm{Ca}}{\lambda^2\exp(2\xi)}, \qquad [15]$$

while the boundary conditions to be satisfied become

$$\varphi = 90°, \quad \text{at the channel centre } \left[\xi = \xi_c = \ln\left(\frac{a}{\lambda}\right)\right], \qquad [16a]$$

and

$$\varphi = \varphi_0, \quad \text{at "the wall" } (\xi = 0), \qquad [16b]$$

where a denotes the half-width of the channel and the appropriate values of φ_0 and λ in any given system are at present unknown. Equation [15] is now written as two first-order differential equations:

$$\frac{\mathrm{d}\varphi}{\mathrm{d}\xi} = \eta \qquad [17]$$

and

$$\frac{\mathrm{d}\eta}{\mathrm{d}\xi} = -\mathrm{Ca}\,A(\varphi) + \eta - \frac{\eta^2}{\tan\varphi}. \qquad [18]$$

Equations [17] and [18] are integrated numerically in parallel using a second-order finite-difference scheme and proceeding from assigned values of φ and η at either the wall or the centre plane of the channel. The step size is automatically adjusted to keep the truncation errors in the values of $\Delta\eta$ and $\Delta\varphi$ below any required value (typically 10^{-3}%). The initial value of η is then adjusted in iterative integrations to satisfy the condition at the second boundary. In figure 4 three solutions of the meniscus equation [7] are presented (Ca = 0.1). When integrating from the wall outward it is seen from curves 1 and 2, with initial η_0-values of 0.256828 and 0.256840, that the shape of the meniscus far from the wall is highly sensitive to the initial value of η_0. When integrating towards the wall it appears from curves 1 and 3, with initial η_c-values of -0.5 and -0.49, that the meniscus shape is much less sensitive to the initial η_c-value. Although the relative difference between the initial values of η is much greater in the latter case than in the preceding one, the difference in the

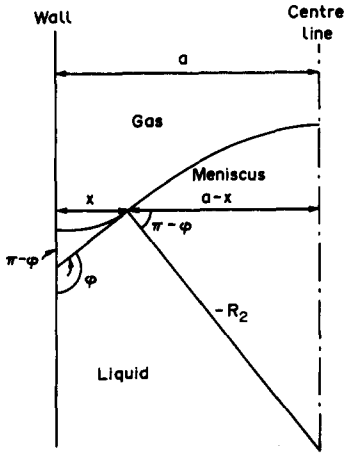

Figure 3. Advancing meniscus in a capillary of radius a.

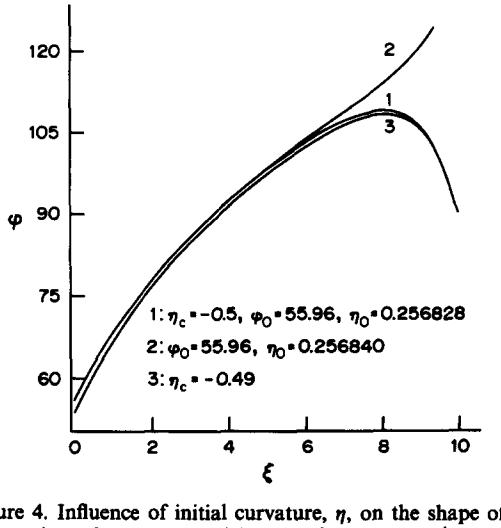

Figure 4. Influence of initial curvature, η, on the shape of the meniscus between parallel plates for $\mathrm{Ca} = 10^{-1}$ (η_0—curvature at the wall, η_c—curvature at the centre).

shape of the meniscus is smaller, corresponding to a difference in φ_0 of only 2°. It can be concluded that the shape of a moving meniscus close to a contact line is rather insensitive to the exact outer boundary conditions. This point is discussed further in section 10.

5. THE NUMERICAL SOLUTION OF THE MENISCUS EQUATION IN THE AXI-SYMMETRIC CASE

Using, again, the logarithmic scale, [13] becomes

$$\frac{\mathrm{d}}{\lambda \exp\xi \,\mathrm{d}\xi}\left[\sin\varphi \frac{\mathrm{d}\varphi}{\lambda \exp\xi \,\mathrm{d}\xi} + \frac{\cos\varphi}{\lambda(\exp\xi_c - \exp\xi)}\right] = \frac{-\mathrm{Ca}\, A(\varphi)\sin\varphi}{\lambda^2 \exp(2\xi)}. \quad [19]$$

This differential equation, describing an advancing meniscus in a tube, can again be written as two first-order differential equations:

$$\frac{\mathrm{d}\varphi}{\mathrm{d}\xi} = \eta \quad [20]$$

and

$$\frac{\mathrm{d}\eta}{\mathrm{d}\xi} = -\mathrm{Ca}\, A(\varphi) + \eta - \frac{\eta^2}{\tan\varphi} + \frac{\eta \exp\xi}{\exp\xi_c - \exp\xi} - \frac{\exp(2\xi)}{\tan\varphi}\frac{1}{(\exp\xi_c - \exp\xi)^2}. \quad [21]$$

These equations are integrated numerically as in the plane case. The results obtained are compared below with the complete numerical solutions of Lowndes (1980).

The numerical solution in the tube geometry is furthermore compared with the corresponding solution in the plate geometry (figure 5). The difference is very small in this case where Ca = 1. For smaller Ca-values the differences may be expected to be still smaller, and for Ca = 0 there will be no difference.

6. COMPARISON WITH COMPLETE NUMERICAL SOLUTIONS

The shape of an advancing meniscus in a capillary has been computed for a number of cases by Lowndes (1980) using a finite-element method. In figure 6 the largest-Ca case treated by Lowndes is compared with the results obtained by integration of [19] from the tube axis to the wall. The value of η at the axis has been chosen to optimize the agreement with the results obtained by Lowndes.

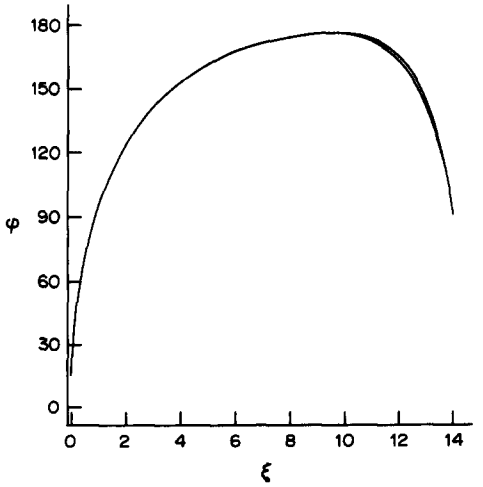

Figure 5. Comparison of the meniscus profiles in the tube and parallel-plate cases (Ca = 1, $\xi_c = 14$, $\varphi_0 = 0°$).

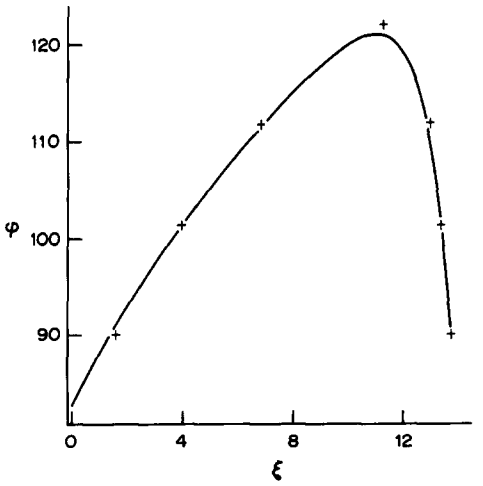

Figure 6. Comparison of the solution of the axi-symmetric meniscus equation [13] (———) with the results obtained by Lowndes (+) for the highest Ca investigated (Ca = $7.53 \cdot 10^{-2}$).

Before commenting on the comparison, a word must be said about the boundary conditions used by Lowndes. As noted earlier, Lowndes assumed the continuum and surface-tension approximations to be valid up to the solid surface ($x = 0$) but the liquid–solid no-slip approximation to break down at a distance (the "slip length") of order 10^{-9} m from the contact line. At values of x less than or of the order of the slip length the solution obtained by Lowndes may therefore be expected to deviate appreciably from that based on a no-slip condition and, accordingly, agreement with the meniscus equation [19] is no longer to be expected. For this reason, λ was chosen for the purposes of comparison to be 10^{-9} m, resulting in a ξ_c-value of 13.79 for the tube concerned ($a = 0.978$ mm).

The two meniscus shapes are in good agreement, with maximum differences of the order of 1°. In the smaller-Ca cases of Lowndes the similarity is comparable or better.

The preliminary conclusion is therefore that the local-wedge approximation looks very promising, implying that the requirement [9] is satisfied. This is broadly confirmed by the results obtained which indicate that the dimensionless wedge-angle variation rate, $|(d\varphi/\varphi)/(ds/w)|$, is $\ll 1$ over the greater part of the meniscus for all values of Ca (figure 7). Very close to the wall the local-wedge approximation is evidently poor for moderate or large Ca. However, this region constitutes only a small part of the zone in which the meniscus is seriously perturbed from the spherical. Very close to the axis, the wedge approximation is also poor but this is immaterial except at large Ca, viscous stresses in this region being negligible anyway. The problem of modelling the central region at large Ca is discussed in section 9.

7. APPROXIMATE ANALYTICAL SOLUTION OF THE MENISCUS EQUATION IN THE WALL REGION

As the wall is approached the plane meniscus equation [7] must always become a good approximation, whether the system geometry is plane or not. This follows from the continual decrease in pressure implied by [5], requiring a corresponding increase in curvature in the plane of flow, that in the perpendicular plane being limited to values less than, or of the order of, the reciprocal of the system length scale, [12].

In the present section an approximate analytical solution of [7] is derived for this region, inspired by its solution in two limiting cases. The first and most obvious of these cases is that of small Ca when the meniscus deviates only slightly from a plane wedge and perturbation approaches are applicable. An analysis of the error in this approximation, however, provides a clue to the second case: that of large φ-values. Both solutions, furthermore, prove to be covered by the same expression.

The final step is to adopt this expression as an approximate solution in *all* cases, the reasoning being as follows. Large values of Ca provoke large values of φ over most of the wall region so that the large-φ solution is likely to provide a good approximation in this case too. This means, however, that a single expression provides a good approximation in both the large- and small-Ca limits and this expression is then likely to be a good approximation in the intermediate-Ca range as well.

Clearly, the final test is a comparison of the analytical approximation with exact solutions of [7] in the wall region and this test is carried out after the derivations concerned.

The small-Ca limit

Equation [7] is based on [5], which gives the pressure, p, in the wall region as

$$p(x) = \int_{\chi=x}^{\chi=x_t} \frac{dp}{d\chi} \cdot d\chi + p_t = \int_x^{x_t} \frac{\mu U A(\varphi)\sin\varphi}{\chi^2} \cdot d\chi + p_t, \qquad [22]$$

where x_t denotes the largest value of x at which [7] is still an adequate approximation and p_t is the corresponding pressure. In view of the strong χ-dependence of the integrand only the region close to $\chi = x$ contributes strongly to the integral and for sufficiently small values of Ca, φ is virtually constant there. In the small-Ca limit, [22] therefore simplifies to

$$p(x) = -\mu U A(\varphi)\sin\varphi\left(\frac{1}{x} - \frac{1}{x_t}\right) + p_t, \qquad [23]$$

which in turn simplifies to

$$p(x) = \frac{-\mu U A(\varphi)\sin\varphi}{x} \qquad [24]$$

for sufficiently small x.

Combination of [6] and [24] now leads to

$$\frac{d\varphi}{dx} = \frac{\mathrm{Ca}\, A(\varphi)}{x}, \qquad [25]$$

a result also derived by Pismen & Nir (1982) [apart from an erroneous minus sign, see Ngan & Dussan (1984)], Hocking & Rivers (1982) and Cox (1986).

The general solution of [25] may be written

$$P(\varphi) = \mathrm{Ca} \ln x + \mathrm{const}, \qquad [26]$$

where

$$P(\varphi) = \int \frac{1}{A(\varphi)} d\varphi. \qquad [27]$$

A series solution is obtainable for $P(\varphi)$ (Bronshtein & Semendyayev 1973):

$$P(\varphi) = \frac{(\varphi - \sin\varphi)}{2} + \frac{\varphi}{2} \ln \frac{\tan\left(\frac{\varphi}{2}\right)}{\frac{\varphi}{2}} - \sum_{n=1}^{\infty} 2^{2n} \frac{(2^{2n-1}-1)}{(2n+1)!n} \cdot \mathrm{B}_n \cdot \left(\frac{\varphi}{2}\right)^{2n+1}, \qquad [28]$$

where B_n denotes the Bernoulli number,

$$\mathrm{B}_n = \frac{2n!}{2^{2n-1}\pi^{2n}} \sum_{k=1}^{\infty} k^{-2n} \qquad [29]$$

($B_1 = 1/6$, $B_2 = 1/30$, $B_3 = 1/42, \ldots$). The region of convergence of [28] is $[0, \pi]$. It is worth noting that useful approximations to the functions $A(\varphi)$ and $P(\varphi)$ are provided by their small-φ limits:

$$A(\varphi) \to 3/\varphi^2, \quad P(\varphi) \to \varphi^3/9; \quad \text{if } \varphi \to 0. \qquad [30]$$

As table 1 shows, these approximations are in practice good ones up to φ-values of about 150°!

Regime of validity

An indication of the error in the above, small-Ca solution for the meniscus shape is provided by the departure from unity, ϵ, of the ratio of the left- and right-hand members of [7], if [25] is inserted for $d\varphi/dx$:

$$\epsilon = \frac{1}{A(\varphi)\sin\varphi} \cdot \frac{\frac{d}{dx}\left(\sin\varphi \frac{d\varphi}{dx}\right)}{\left(\frac{-\mathrm{Ca}}{x^2}\right)} - 1 \qquad [31]$$

$$= \frac{-x^2}{\sin\varphi A(\varphi)} \cdot \frac{d}{dx}\left[\frac{\sin\varphi A(\varphi)}{x}\right] - 1 \qquad [32]$$

$$= \frac{-x}{\sin\varphi A(\varphi)} \cdot \frac{d[\sin\varphi A(\varphi)]}{d\varphi} \cdot \frac{d\varphi}{dx} \qquad [33]$$

$$= \frac{-\mathrm{Ca}}{\sin\varphi} \cdot \frac{d[\sin\varphi A(\varphi)]}{d\varphi},$$

which, making use of [3], may be written

$$\epsilon = \mathrm{Ca}\, E(\varphi), \qquad [34]$$

Table 1. Accuracy of approximations [30]

φ	$\varphi^2 A(\varphi)/3$	$9P(\varphi)/\varphi^3$
0	1	1
$\pi/4$	1.02	0.99
$\pi/2$	1.05	0.97
$3\pi/4$	0.92	0.99
$5\pi/6$	0.75	1.05
$11\pi/12$	0.46	1.20
π	0	∞

Table 2. Applicability of approximations [37] and [38]

φ	$E(\varphi)$	$\varphi^3 E(\varphi)/3$	$\pi E(\varphi)/4$
0	∞	1	∞
$\pi/4$	7.45	1.203	5.85
$\pi/2$	1.621	2.094	1.273
$3\pi/4$	1.164	5.075	0.914
π	1.273	13.16	1

where

$$E(\varphi) = A(\varphi)[A(\varphi)\sin\varphi - 2\cot\varphi]. \qquad [35]$$

Evidently the small-Ca solution should provide a good approximation provided

$$\mathrm{Ca}\, E(\varphi) \ll 1. \qquad [36]$$

The large-φ limit

The function $E(\varphi)$ possesses simple small- and large-φ limits (table 2):

$$E(\varphi) \to 3/\varphi^3, \quad \varphi \to 0 \qquad [37]$$

and

$$E(\varphi) \to 4/\pi, \quad \varphi \to \pi. \qquad [38]$$

For large φ, $E(\varphi)$ is constant and, consequently, also ϵ. This provides the clue to a large-φ solution of [7], of the same form as [26] but with Ca replaced by a function of itself, Ca′ (see [31]):

$$P(\varphi) = \mathrm{Ca}' \ln x + \text{const.} \qquad [39]$$

The function Ca′ is found by inserting the differential form of [39],

$$\frac{\mathrm{d}\varphi}{\mathrm{d}x} = \frac{\mathrm{Ca}'\, A(\varphi)}{x}, \qquad [40]$$

into [7]. The result is

$$\mathrm{Ca}'\left\{-1 + \mathrm{Ca}' \frac{1}{\sin\varphi}\frac{\mathrm{d}}{\mathrm{d}\varphi}\left[A(\varphi)\sin\varphi\right]\right\} = -\mathrm{Ca} \qquad [41]$$

or

$$\mathrm{Ca}'[-1 - \mathrm{Ca}'\, E(\varphi)] = -\mathrm{Ca}. \qquad [42]$$

For large φ, [42] is

$$\mathrm{Ca}' = \frac{\pi}{8}\left[-1 \pm \left(1 + \frac{16\,\mathrm{Ca}}{\pi}\right)^{1/2}\right]. \qquad [43]$$

Since

$$\mathrm{Ca}' \to \mathrm{Ca}, \quad \text{if } \mathrm{Ca} \to 0, \qquad [44]$$

the positive root applies:

$$\mathrm{Ca}' = \frac{\pi}{8}\left[\left(1 + \frac{16\,\mathrm{Ca}}{\pi}\right)^{1/2} - 1\right]. \qquad [45]$$

General approximation

As discussed earlier, [39] covers both the large-φ and small-Ca limits (in the latter case Ca′→Ca and, consequently, [39]→[26]) and is a candidate for a generally applicable solution

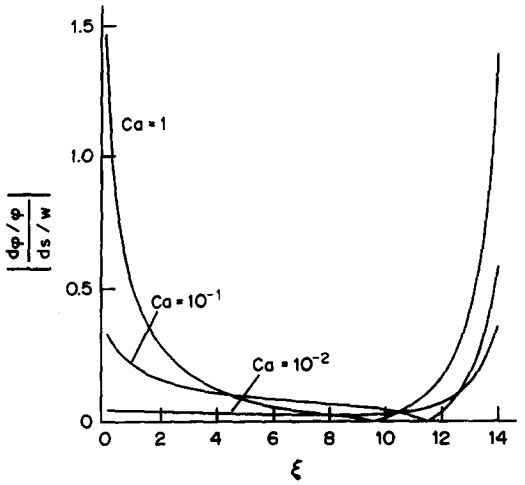

Figure 7. The dimensionless wedge-angle variation rate $|(d\varphi/\varphi)/(ds/w)|$ as a function of ξ for $Ca = 1$, 10^{-1} and 10^{-2} ($\xi_c = 14$ and $\varphi_0 = 45°$).

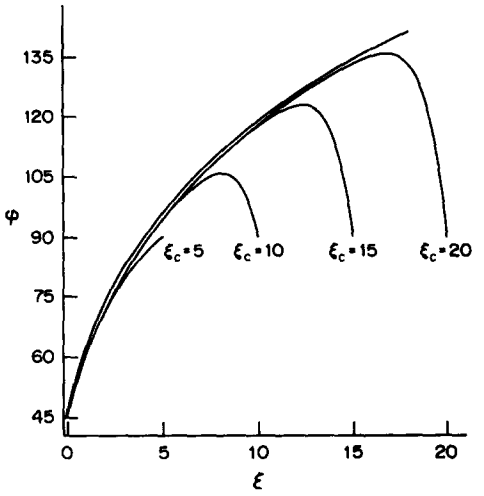

Figure 8. Comparison of the analytical approximation of the meniscus equation [13] with the exact solution for $\xi_c = 5$, 10, 15 and 20 ($Ca = 10^{-1}$, $\varphi_0 = 45°$). The analytical approximation is the uppermost curve.

to [7] in the wall region. Application of the boundary condition [16b] yields the final form of the equation:

$$P(\varphi) - P(\varphi_0) = Ca' \ln\left(\frac{x}{\lambda}\right). \qquad [46]$$

Comparison with the exact solutions of the meniscus equation

To indicate the accuracy of approximation [46], a number of comparisons with numerical solutions of [7] and [13] are presented in the axi-symmetric case.

In figure 8 the model is compared with four numerical solutions (where $\xi_c = 5$, 10, 15 and 20) for moderate values of Ca and φ_0, $Ca = 10^{-1}$ and $\varphi_0 = 45°$. In the wall region the model describes the meniscus shape within about 2°. The effect of higher or lower Ca-values is examined in figures 9 and 10 ($Ca = 1$ and $Ca = 10^{-2}$, respectively). If anything, the agreement is better. Finally, larger and smaller φ_0-values are examined in figures 11 and 12 ($\varphi_0 = 0°$ and $\varphi_0 = 90°$,

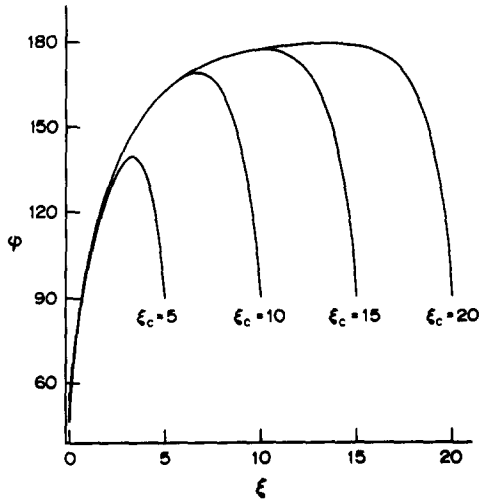

Figure 9. Comparison of the analytical approximation of the meniscus equation [13] with the exact solution for $\xi_c = 5$, 10, 15 and 20 ($Ca = 1$, $\varphi_0 = 45°$). In the wall region the analytical approximation is indistinguishable from the exact solutions.

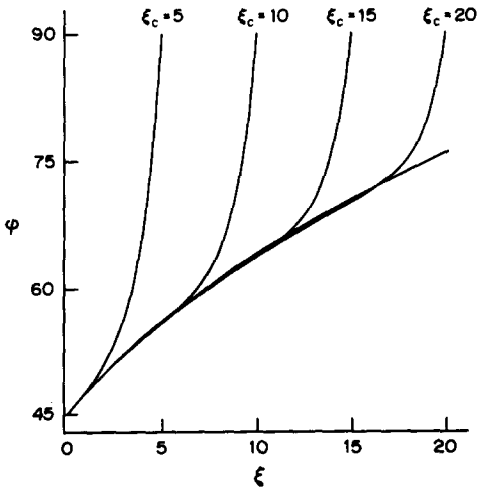

Figure 10. Comparison of the analytical approximation of the meniscus equation [13] with the exact solution for $\xi_c = 5$, 10, 15 and 20 ($Ca = 10^{-2}$, $\varphi_0 = 45°$).

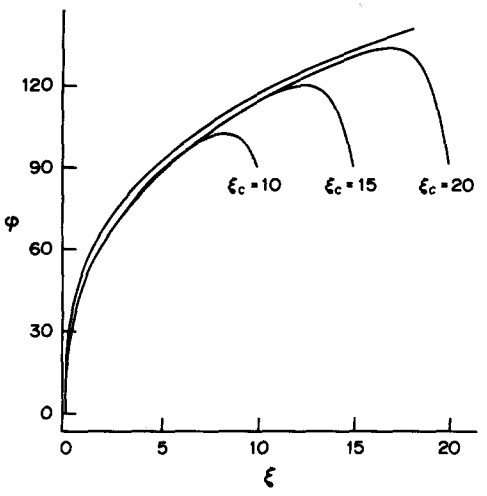

Figure 11. Comparison of the analytical approximation of the meniscus equation [13] with the exact solution for $\xi_c = 5$, 10, 15 and 20 ($Ca = 10^{-1}$, $\varphi_0 = 0°$).

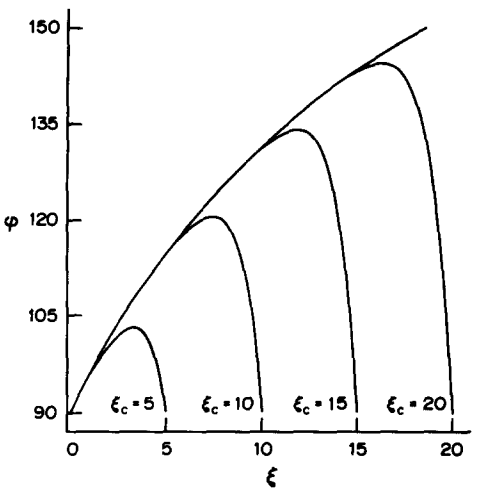

Figure 12. Comparison of the analytical approximation of the meniscus equation [13] with the exact solution for $\xi_c = 5$, 10, 15 and 20 ($Ca = 10^{-1}$, $\varphi_0 = 90°$).

respectively). For $\varphi_0 = 0°$ the agreement is only to within about 7°, but for $\varphi_0 = 90°$ the differences are minimal.

8. ANALYTICAL APPROXIMATION FOR THE ENTIRE MENISCUS

The central region

In the central region of the meniscus the viscous stresses are of order $\mu U/a$, while the pressure difference between the liquid and gas is of order σ/a. Provided the ratio of these terms, Ca, is small, the central portion of the meniscus should have a very nearly spherical profile. The observations of Hoffman (1975) for capillary tubes confirm this expectation, surprisingly even for $Ca > 1$. The explanation of the latter fact probably lies in the viscous (deviatoric) contribution to the stress at the free surface which is negligible in the wall region (section 2) but *not* at the tube axis. This additional contribution will offset that due to pressure variation. Whatever the explanation, however, the result is useful and the next task consists of matching this central, circular profile to the wall solution [46].

Matching of the wall and central region

If, consistent with the preceding considerations, viscous normal stresses are neglected in the central region, the meniscus equation for the entire region may be written as

$$-\sigma\left(\frac{1}{R_1}+\frac{1}{R_2}\right)=p_v+p_c, \qquad [47]$$

where p_c denotes the constant pressure in the central region and p_v is the additional pressure due to viscous stresses. In the central region the term p_v may be neglected, while in the wall region this term dominates and R_2^{-1} and p_c may be neglected. In the transition region all terms are clearly significant.

The simplest matching procedure is to ignore the transition region and treat the central and wall approximations as valid up to some transition value of x, x_t. The optimal choice of the transition point is clearly that at which the errors in the respective approximations are equal, i.e. where

$$\left|p_c+\frac{\sigma}{R_2}\right|=|p_v|. \qquad [48]$$

For the tube geometry, R_2 is given at x_t by $\cos\varphi_t/(a-x_t)$. Consequently, $p_c=-2\sigma\cos\varphi_t/(a-x_t)$ and

$$\left|p_c+\frac{\sigma}{R_2}\right|=\left|\frac{\sigma\cos\varphi_t}{a-x_t}\right|. \tag{49}$$

Equation [49] also applies to the parallel-plate system since then $R_2=\infty$ and $p_c=-\sigma\cos\varphi_t/(a-x_t)$. An expression for p_v is obtained from the relations for the wall solution, [6] and [40]:

$$-p_v=\sigma\sin\varphi_t\frac{\mathrm{Ca}'A(\varphi)}{x_t}. \tag{50}$$

Making use of [49] and [50], [48] yields the transition criterion:

$$\frac{x_t}{a}=\frac{\mathrm{Ca}'A(\varphi_t)|\tan\varphi_t|}{1+\mathrm{Ca}'A(\varphi_t)|\tan\varphi_t|}. \tag{51}$$

Substitution of [51] into the solution for the wall region, [46] gives

$$P(\varphi_t)=P(\varphi_0)+\mathrm{Ca}'\ln\left[\frac{a}{\lambda}\cdot\frac{\mathrm{Ca}'A(\varphi_t)|\tan\varphi_t|}{1+\mathrm{Ca}'A(\varphi_t)|\tan\varphi_t|}\right]. \tag{52}$$

Given φ_0, [52] can be solved iteratively to obtain φ_t and hence, via [51], x_t.

The dynamic contact angle

Defining the dynamic (apparent) contact angle φ_d as the angle obtained by extrapolating the circular profile in the external region to the wall, φ_d is obtained from φ_t and x_t by means of the relation

$$\cos\varphi_d=\frac{\cos\varphi_t}{1-\dfrac{x_t}{a}}. \tag{53}$$

Consistent with the definition of φ_d in the analytical case, in the numerical case φ_d was taken as the angle obtained if the curvature at the tube axis were to persist up to the wall:

$$\varphi_d=\arctan\left[\left(\frac{1}{\eta_c^2}-1\right)^{1/2}\right], \tag{54}$$

for $\eta_c>0$; and

$$\varphi_d=180^\circ-\arctan\left[\left(\frac{1}{\eta_c^2}-1\right)^{1/2}\right], \tag{55}$$

for $\eta_c<0$.

9. COMPARISON WITH EXPERIMENTAL RESULTS

The required boundary conditions at the wall

A comparison of the models developed above with measurements of φ_d is clearly possible only if values of φ_0 and λ can be specified. Ideally λ should be assigned a value larger than the range of intermolecular forces ($\cong 10^3$ Å) but much smaller than the system length scale, a. As pointed out by Kafka & Dussan (1979), the corresponding value of φ_0 should then be a material property in the sense that it depends only on the line speed for the given media. No data on such functional dependence of this value of φ_0 on U exist, however, and some plausible alternative must therefore be sought.

The simplest model, adopted here, is to suppose that the various classical approximations—the continuum and no-slip approximations and the idealization of a surface tension—retain their validity down to a distance from the wall of the order of a molecular dimension, at which point the true contact angle is attained (this concept having no meaning at submolecular distances). One result of this incorporation of the molecular nature of the liquid is that the much discussed stress

singularity at the contact line does not arise. As discussed earlier, other authors have avoided this singularity by retaining the continuum approximation and assuming the no-slip approximation to lose its validity close to the contact line. However, the "slip length" required to obtain agreement with observed values of φ_d then proves to be of the order of a molecular dimension (Lowndes 1980), which both undermines the credibility of the continuum treatment and points to a molecular explanation. Though unknown to the authors at the time, this approach has also been followed by Voinov (1976, 1978).

To complete the boundary conditions at the wall, the true contact angle there is assumed to be sufficiently approximated by the static value

$$\varphi_0 = \varphi_s. \qquad [56]$$

This assumption has been made by most authors, though Hoffman (1983) has presented arguments for substantial Ca-dependence of the true contact angle. At the large values of Ca at which the difference between φ_0 and φ_s is likely to become appreciable, however, the value of φ_d predicted by [51]–[53] depends only weakly on φ_0. Numerically obtained results of φ_d vs φ_0 for a few Ca-values are shown in figure 13 for $\xi_c = 14$. The validity of approximation [56] is thus less crucial to the prediction of φ_d than it would at first sight appear. (Conversely, good agreement between observations and predictions based on approximation [56] furnishes no proof of the accuracy of this approximation!)

Comparisons

The values of the dynamic contact angle predicted by the analytical approximation [51]–[53] and those obtained by numerical solution of the meniscus equation [13] can now be compared with those found experimentally in tubes [Hoffman (1975) and corroborated by Fermigier & Jenffer (1988)].

The resulting comparisons are set out in figures 14–17 for a λ-value of 1 nm. While the best-fit value of this length scale cannot be specified to better than a factor of 5 or so, it is certainly of the order of a molecular dimension.

At $Ca < 10^{-1}$, both models are seen to agree well with the experimental results. For larger Ca, the analytical approximation continues to provide an excellent prediction while, paradoxically, the model based on the neglect of fewer terms fails. On reflection this result is understandable. Both models are reliable in the wall region. In the central region, however, the analytical approximation assumes a circular profile which, as discussed in section 8, somewhat fortuitously proves to be a better approximation than that obtained taking account of pressure variation but neglecting viscous normal stresses.

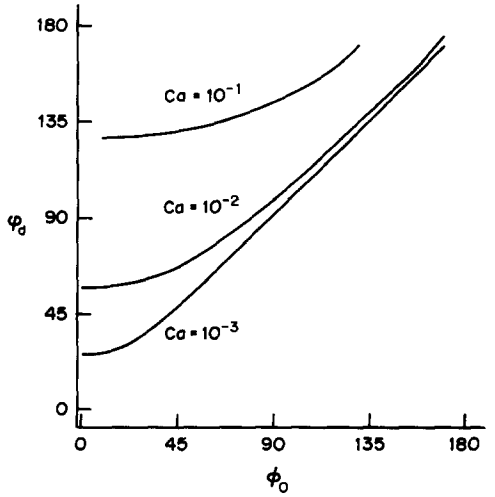

Figure 13. The dependence of the dynamic contact angle on the true contact angle at the wall for various Ca ($\xi_c = 14$).

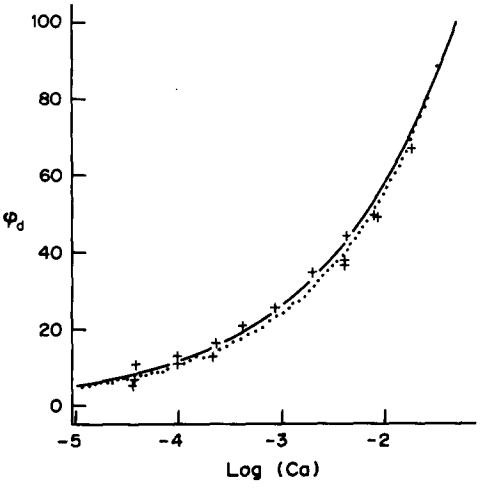

Figure 14. Ca-dependence of the dynamic contact angle as measured by Hoffman (+), as predicted by the analytical approximation equations [51]–[53] (· · · · ·) and as predicted by the meniscus equation [13] (———). The liquid used in Hoffman's experiments was G. E. Silicone Fluid SF-96 ($\mu = 0.958\ \mathrm{kg\,m^{-1}\,s^{-1}}$, $\sigma = 2.13 \cdot 10^{-2}\ \mathrm{N\,m^{-1}}$, static contact angle = 0°).

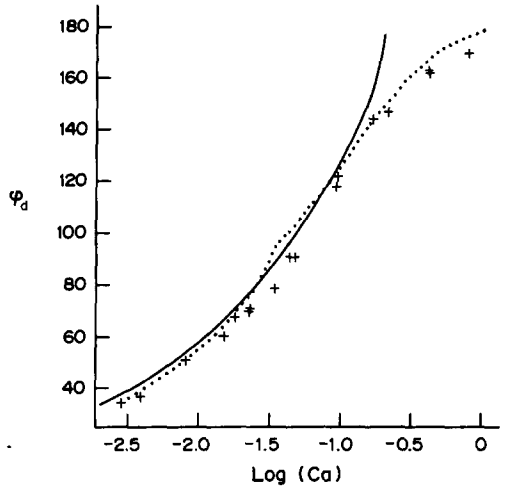

Figure 15. Ca-dependence of the dynamic contact angle as measured by Hoffman (+), as predicted by the analytical approximation equations [51]–[53] (· · · · ·) and as predicted by the meniscus equation [13] (———). The liquid used in Hoffman's experiments was Brookfield Std. Viscosity Fluid ($\mu = 98.8\,\mathrm{kg\,m^{-1}\,s^{-1}}$, $\sigma = 2.17 \cdot 10^{-2}\,\mathrm{N\,m^{-1}}$, static contact angle = 0°).

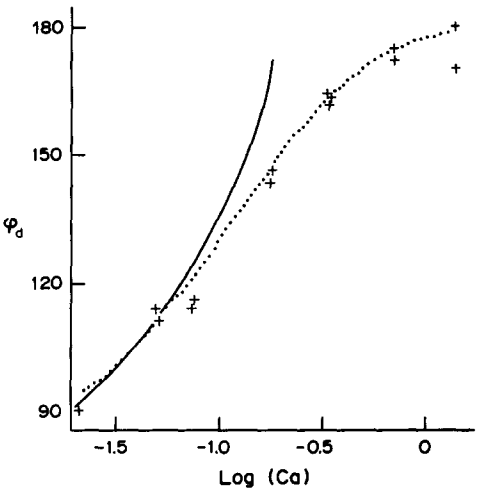

Figure 16. Ca-dependence of the dynamic contact angle as measured by Hoffman (+), as predicted by the analytical approximation equations [51]–[53] (· · · · ·) and as predicted by the meniscus equation [13] (———). The liquid used in Hoffman's experiments was Ashland Chem. Admex 760 ($\mu = 109.3\,\mathrm{kg\,m^{-1}\,s^{-1}}$, $\sigma = 4.38 \cdot 10^{-2}\,\mathrm{N\,m^{-1}}$, static contact angle = 69°).

10. SYSTEM-DEPENDENCE OF THE DYNAMIC CONTACT ANGLE

The minor influence of system geometry on meniscus shape (and, by implication, on dynamic contact angle) has been illustrated in figure 5. The effect of system *scale*, a, is reflected, for a given geometry, in the influence of $\xi_c (= \ln(a/\lambda))$. Figure 18 illustrates the fact that the dependence of the dynamic contact angle on the system scale is similarly weak. The case $\varphi_0 = 90°$ has been chosen to allow a comparison with the small-Ca prediction of Kafka & Dussan (1979).

The figure equally demonstrates the weak dependence, for a given system, of the dynamic contact angle on the length scale λ.

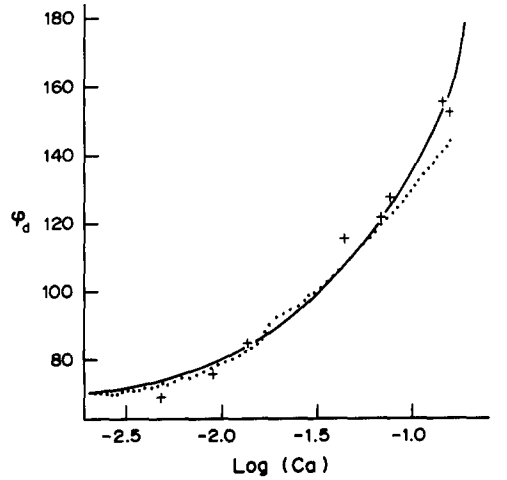

Figure 17. Ca-dependence of the dynamic contact angle as measured by Hoffman (+), as predicted by the analytical approximation equations [51]–[53] (· · · · ·) and as predicted by the meniscus equation [13] (———). The liquid used in Hoffman's experiments was Santicizer 405 ($\mu = 11.2\,\mathrm{kg\,m^{-1}\,s^{-1}}$, $\sigma = 4.34 \cdot 10^{-2}\,\mathrm{N\,m^{-1}}$, static contact angle = 67°).

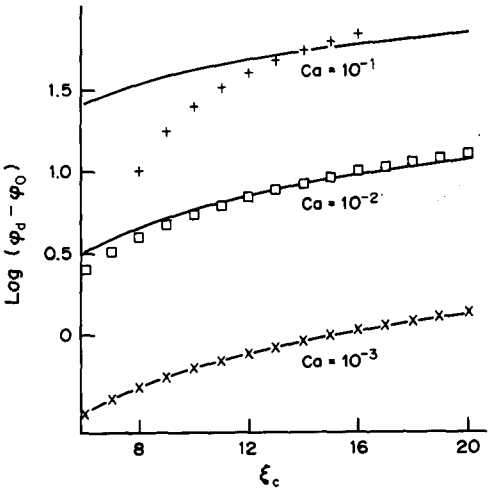

Figure 18. The dependence of the dynamic contact angle on the system scale (represented by ξ_c) as predicted by meniscus equation [13] (———) and by Kafka & Dussan (symbols), for various Ca and $\varphi_0 = 90°$. At $\xi_c = 14$ both models are made to agree.

11. CONCLUSIONS AND FINAL DISCUSSION

An alternative to full numerical solution of the flow and meniscus shape associated with an advancing liquid–gas contact line has been explored, based on a local-wedge approximation. Up to $Ca \approx 10^{-1}$ the associated errors are acceptable over the entire meniscus, as supported by the excellent agreement with available numerical solutions. At higher Ca, for which viscous stresses become significant in the central region of the meniscus, only the wall region is adequately described by the approximation. Good agreement with measured values of the advancing contact angle is nevertheless obtained if the wall profile is matched to a circular central profile. This leads to an analytical approximation for the dynamic contact angle, applicable at all.

Since the local-wedge approximation involves no assumption as to the sign of the line speed it should be applicable in the liquid–gas *receding* case and can probably be extended to the liquid–liquid case also (which involves both advancing and receding liquids). Indeed, in these cases Ca-values are likely to be limited to order 10^{-1} or less, a film of the receding liquid being left behind at larger Ca.

The question of the appropriate boundary conditions at the solid surface remains unsettled, the only contribution of the present work being to demonstrate that boundary conditions taking account of the discontinuous nature of the liquid but retaining the no-slip approximation are as successful in removing the wall singularity and in predicting the dynamic contact angle as are the reverse assumptions. However, neither these assumptions nor that of constant true contact angle are severely tested in the advancing case, the predicted dynamic angle being relatively insensitive to conditions at the wall. It is noteworthy that this will not be so if the liquid is receding and comparisons of predictions and experiment in this case should be highly illuminating.

Finally, we note that the model developed predicts a weak system-dependence of the dynamic contact angle (e.g. tube-radius-dependence: [51]–[53]) which cannot, as noted by Kafka & Dussan (1979), be viewed as a material property.

REFERENCES

BRONSHTEIN, I. N. & SEMANDYAYEV, K. A. 1973 *A Guide Book to Mathematics.* Verlag Harri Deutsch/Springer-Verlag, Berlin.

COX, R. G. 1986 The dynamics of the spreading of liquids on a solid surface. Part 1. Viscous flow. *J. Fluid Mech.* **168,** 169–194.

DUSSAN, V. E. B. 1979 On the spreading of liquids on solid surfaces: static and dynamic contact lines. *A. Rev. Fluid Mech.* **11,** 371–400.

FERMIGIER, M. & JENFFER, P. 1988 Dynamics of a liquid–liquid interface in a capillary. *Annls Phys.* **13** (2), 37–42.

DE GENNES, P. G. 1985 Wetting: statics and dynamics. *Rev. mod. Phys.* **57,** 827–863.

GREENSPAN, H. P. 1978 On the motion of a small viscous droplet that wets a surface. *J. Fluid Mech.* **84,** 125–143.

HANSEN, R. J. & TOONG, T. Y. 1971 Dynamic contact angle and its relationship to forces of hydrodynamic origin. *J. Colloid Interface Sci.* **37,** 196–207.

HOCKING, L. M. & RIVERS, A. D. 1982 The spreading of a drop by capillary action. *J. Fluid Mech.* **121,** 425–442.

HOFFMAN, R. L. 1975 A study of the advancing interface I. Interface shape in liquid–gas systems. *J. Colloid Interface Sci.* **50,** 228–241.

HOFFMAN, R. L. 1983 A study of the advancing interface II. Theoretical prediction of the dynamic contact angle in liquid–gas systems. *J. Colloid Interface Sci.* **94,** 470–486.

HUH, C. & MASON, S. G. 1977 The steady movement of a liquid meniscus in a capillary tube. *J. Fluid Mech.* **81,** 401–419.

KAFKA, F. Y. & DUSSAN, V. E. B. 1979 On the interpretation of dynamic contact angles in capillaries. *J. Fluid Mech.* **95,** 539–565.

LOWNDES, J. 1980 The numerical simulation of the steady movement of a fluid meniscus in a capillary tube. *J. Fluid Mech.* **101,** 631–646.

MOFFATT, H. K. 1964 Viscous and resistive eddies near a sharp corner. *J. Fluid Mech.* **18,** 1–18.

NEOGI, P. & MILLER, C. A. 1982 Spreading kinetics of a drop on a smooth solid surface. *J. Colloid Interface Sci.* **86,** 525–538.

NGAN, C. G. & DUSSAN, V. E. B. 1984 The moving contact line with a 180° advancing contact angle. *Phys. Fluids* **27,** 2785–2787.

PISMEN, L. M. & NIR, A. 1982 Motion of a contact line. *Phys. Fluids* **25,** 3–7.

VOINOV, O. V. 1976 Hydrodynamics of wetting. *Fluid Dynam* **11,** 714–721.

VOINOV, O. V. 1978 Asymptote to the free surface of a viscous liquid creeping on a surface and the velocity dependence of the angle of contact. *Sov. Phys. Dokl.* **23,** 891–893.